Study of the uncertainty of angle measurement for a rotary-laser automatic theodolite (R-LAT)

J E Muelaner[1]*, Z Wang[1], J Jamshidi[1], P G Maropoulos[1], A R Mileham[1], E B Hughes[2], and **A B Forbes[2]**
[1]Department of Mechanical Engineering, University of Bath, Bath, UK
[2]National Physical Laboratory, Teddington, UK

The manuscript was received on 23 June 2008 and was accepted after revision for publication on 20 November 2008.

DOI: 10.1243/09544054JEM1272

Abstract: This paper shows how the angular uncertainties can be determined for a rotary-laser automatic theodolite of the type used in (indoor-GPS) iGPS networks. Initially, the fundamental physics of the rotating head device is used to propagate uncertainties using Monte Carlo simulation. This theoretical element of the study shows how the angular uncertainty is affected by internal parameters, the actual values of which are estimated. Experiments are then carried out to determine the actual uncertainty in the azimuth angle. Results are presented that show that uncertainty decreases with sampling duration. Other significant findings are that uncertainty is relatively constant throughout the working volume and that the uncertainty value is not dependent on the size of the reference angle.

Keywords: iGPS, indoor GPS, infrared GPS, constellation 3Di

1 INTRODUCTION

Rotary-laser automatic theodolites (R-LATs) have been used as part of a network of such devices to form a highly adaptable large-scale coordinate measurement machine; this patented [**1**] system is known commercially as iGPS (indoor global positioning system). iGPS has been demonstrated in various applications such as jigless assembly of aircraft structures [**2**], positioning of robots, and the alignment of laser projection [**3**]. There have also been reports of tests in some cases showing results better than those for a laser tracker [**2**]. Rapid, accurate measurements are an important factor in enabling the acquisition of online information about product quality, which could subsequently be used to automatically correct the processes and compensate manufacturing errors [**4**].

Unfortunately, there has been very little work published to independently verify the performance of the iGPS system. Uncertainty in the coordinate measurements given by an iGPS network propagates from the uncertainties in the angular measurements of the individual automatic theodolites. In order to fully understand the uncertainties of the network it is therefore important to first understand and characterize the uncertainties of an individual R-LAT.

An R-LAT is made up of two parts: a transmitter and a sensor. The transmitter consists of a stationary body and a rotating head. The rotating head sweeps two fanned laser beams through the working volume, while the stationary body delivers a strobe with a single pulse for every other revolution of the head. The fanned laser beams are inclined at 30° to the horizontal and offset by 90° to one another [**1**] as shown in Fig. 1.

The sensor is able to detect both the fanned laser beams as they sweep past and the pulse of light from the strobe. There is no other form of communication between the transmitter and receiver. Azimuth and elevation angles are calculated using the timing differences between pulses of light reaching the sensor, as explained in section 3.

In an iGPS network, a point can be located by a single sensor as long as the sensor receives optical signals from at least two different transmitters. Each transmitter is configured to rotate at a slightly different speed, typically approximately 3000 r/min. It is this difference in speed which allows the system to differentiate between the signals from different transmitters [**1**].

**Corresponding author: Department of Mechanical Engineering, University of Bath, Bath BA2 7AY, UK. email: J.E.Muelaner@bath.ac.uk*

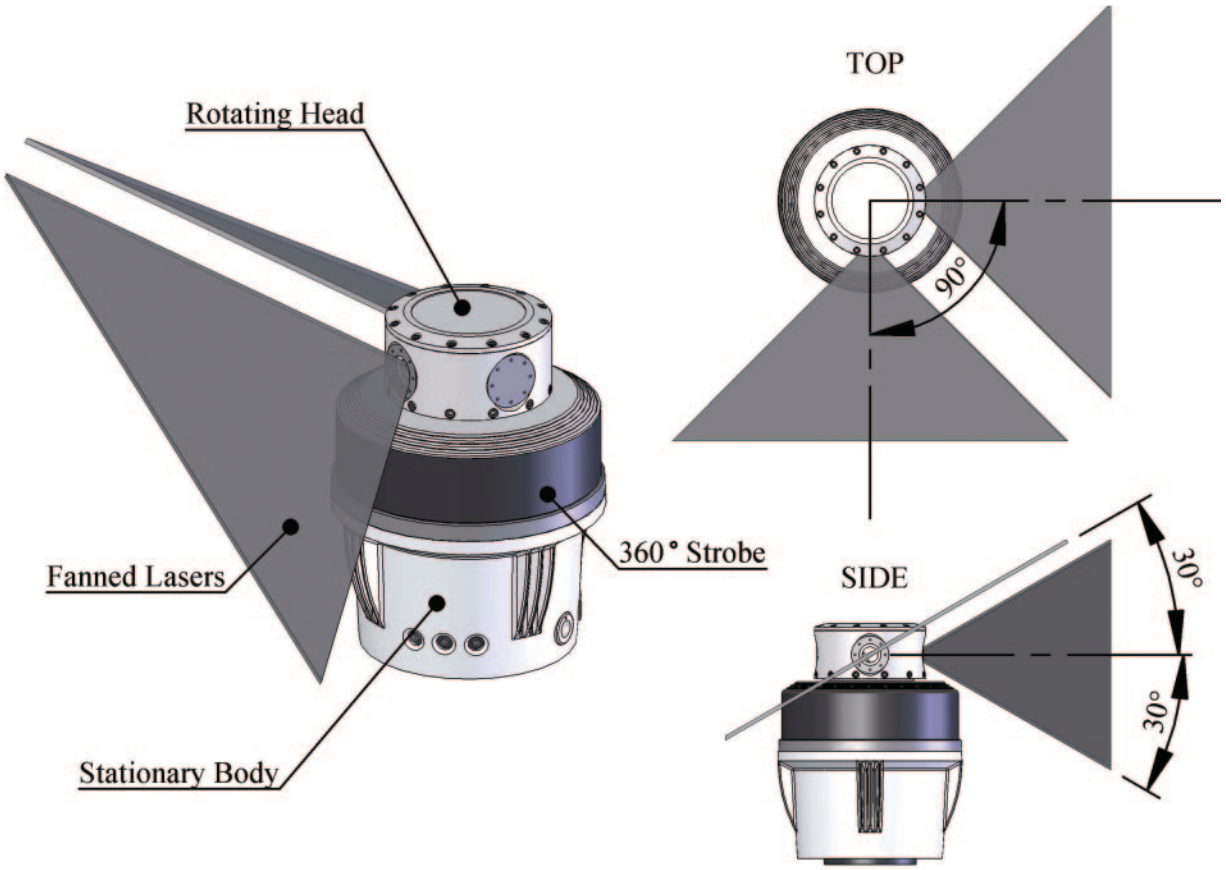

Fig. 1 Main components of the transmitter

iGPS employs triangulation to automatically generate positional measurements at a single receiver based on angle measurements from multiple transmitters. Automatic triangulation has been demonstrated with automatic theodolites [**5**] and with tracking lasers [**6**]. Multilateration also generates positions based on measurements from multiple stations to a single measurement sensor but in this case distances are used rather than angles. This technique is widely used in navigation; Decca and NAVSTAR GPS are both based on multilateration [**7**]. Multilateration has been demonstrated in metrology with specially constructed tracking interferometers [**8**, **9**] and using industrial laser trackers [**10**] in applications such as the assembly of spacecraft structures [**11**]. Perhaps the most similar system to iGPS is the Anglescan positioning system [**12**] which utilizes devices containing a fixed laser which is caused to sweep across the horizon by a rotating mirror. In the Anglescan system the laser is reflected back to the instrument by a retroreflector and the pulse of light is detected at the transmitter. Anglescan is only able to detect azimuth angles and can therefore detect two-dimensional positions for navigation.

A novel aspect of the iGPS system is the use of the R-LATs, described above, which have the following advantages.

1. The one-way communication allows a theoretically unlimited number of sensors to simultaneously detect signals from a single network of transmitters. The iGPS system is therefore massively scalable in a similar way to the NAVSTAR GPS network.
2. Since the transmitters are not required to track as is the case with theodolites and laser trackers, there is no requirement to re-aim the transmitter following a disruption in the line of sight.
3. Unlike the corner cube reflectors used with laser trackers the sensor component of an R-LAT is able to detect signals coming from a wide range of angles, typically 360° in azimuth and at least ±30° in elevation.
4. Benefits 2 and 3 above mean that, assuming there is sufficient redundancy in the network, a sensor can move around various line-of-sight obstructions losing and regaining connection to transmitters with relative ease.

The flexibility of operation facilitated by the system has considerable potential for use within the

aerospace sector and other large-scale manufacturing sectors.

Assuming that the transmitters' positions are known, the position of the sensor can be calculated from the angular measurements using triangulation. A system with more than two transmitters will be able to apply some form of least squares fitting to the redundant data to reduce the uncertainty of the coordinate measurements. The normal setup procedure for an iGPS network includes a bundle adjustment in order to determine the relative positions of the transmitters. Bundle adjustment is suitable for any measurement system employing triangulation [**13**] and has been employed extensively with photogrammetry [**14**, **15**].

2 DEVELOPING A VERIFICATION STRATEGY

There is a large body of literature concerning the verification of coordinate measurements. Of particular importance are the ISO 10360 standard for coordinate measuring machines (CMMs) [**16**] and the ASME B89 standard for laser trackers [**17**]. These share many common practices, most notably low-level tests which isolate subsystems followed by high-level tests which test the combined use of subsystems in more realistic conditions. Such subsystems are the probing error and x, y, z encoders on a CMM, while on a laser tracker they are the two angle encoders, the interferometer, and the probing error of the retro-reflector.

By applying the principle of isolating subsystems we should test the individual R-LAT (transmitter–receiver arrangement) in a similar way to a conventional theodolite. Unfortunately, there is no established standard for the verification of theodolites. The tests contained in the ISO standard for field testing theodolites is used by manufacturers such as Leica in product data sheets [**18**] despite the standard stating that, 'They are not proposed as tests for acceptance or performance evaluations ...' [**19**].

Additional tests would also be required to fully characterize the iGPS system according to the established methodology for testing CMMs. In particular, there should be tests to identify the significance of probing error, and tests for the actual coordinate measurement performance, both in controlled conditions and in realistic measurement tasks. The initial phase of testing was concerned only with the angular performance of the R-LAT and this work is reported in this paper.

3 MATHEMATICAL MODELLING

Consider the two fanned lasers sweeping through the measurement volume and the strobe illuminating the volume. If a vector is located so that it is normal to the first fan when that fan crosses the sensor (at t_1) and a second vector is similarly located so that it is normal to the second fan at t_2 then a third vector which is orthogonal to the first two will give the direction from the transmitter to the target sensor.

Based on the geometry shown in Fig. 2 it is possible to say that the system is capable of measuring any azimuth angle but the range of possible elevation angles is limited by the angles α_1 and α_2. More specifically fan 1 will never intersect with a target which is at an elevation angle greater than $\pi - \alpha_1$ or less than $\alpha_1 - \pi$. Similarly fan 2 will never intersect with a target at an elevation angle greater than α_2 or less than $-\alpha_2$.

If the axis of rotation lies on the z-axis then the normal to the plane of the first fan when this fan is aligned with the x-axis is given by

$$\boldsymbol{n}_{1x} = \begin{bmatrix} 0 \\ -\sin\alpha_1 \\ \cos\alpha_1 \end{bmatrix} \tag{1}$$

Similarly when the second fan is aligned with the x-axis the normal to this plane is given by

$$\boldsymbol{n}_{2x} = \begin{bmatrix} 0 \\ \sin\alpha_2 \\ -\cos\alpha_2 \end{bmatrix} \tag{2}$$

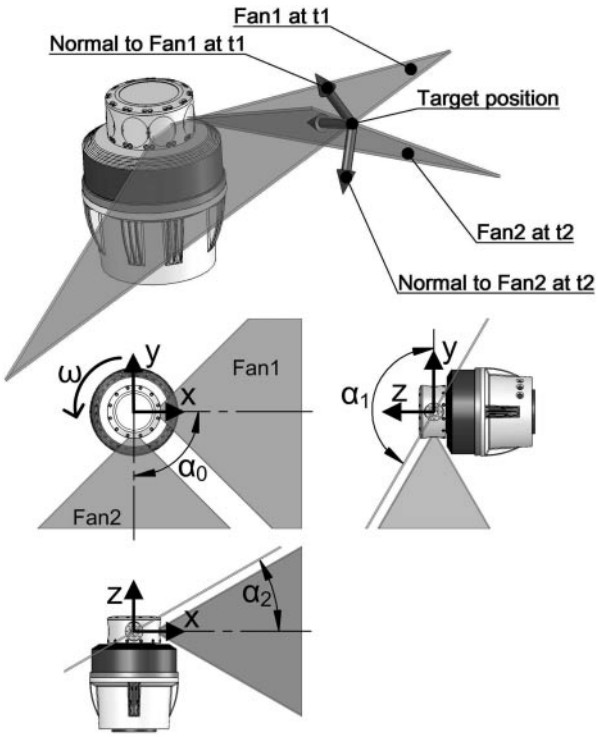

Fig. 2 Angles used in mathematical model

Assuming that the strobe is activated as fan 1 is aligned with the x-axis, at t_1 fan 1 passes the sensor and has rotated about the z-axis through angle

$$a_1 = (t_1 - t_0)\omega \tag{3}$$

Rotating $\boldsymbol{n}_{1x}$ by a_1 gives the vector normal to the first fan at t_1

$$\boldsymbol{n}_{1T} = \begin{bmatrix} \cos a_1 & \sin a_1 & 0 \\ -\sin a_1 & \cos a_1 & 0 \\ 0 & 0 & 1 \end{bmatrix} \times \boldsymbol{n}_{x1} \tag{4}$$

At t_2 as the second fan passes the sensor target and is at an angle relative to alignment with the x-axis given by

$$a_2 = (t_2 - t_0)\omega - \alpha_0 \tag{5}$$

Rotating $\boldsymbol{n}_{2x}$ by a_2 gives the vector normal to the first fan at t_2

$$\boldsymbol{n}_{2T} = \begin{bmatrix} \cos a_2 & \sin a_2 & 0 \\ -\sin a_2 & \cos a_2 & 0 \\ 0 & 0 & 1 \end{bmatrix} \times \boldsymbol{n}_{x2} \tag{6}$$

The target lies on the first fan at t_1 and the second fan at t_2, and the line connecting the origin of the fans with the target must therefore be orthogonal to the two normals with the direction give by

$$\begin{bmatrix} x_1 \\ x_2 \\ x_3 \end{bmatrix} = \boldsymbol{n}_{1T} \times \boldsymbol{n}_{2T} \tag{7}$$

From equation (7) it is straightforward to calculate the azimuth and elevation angles

$$r = \sqrt{\begin{bmatrix} x_1 \\ x_2 \end{bmatrix} \times \begin{bmatrix} x_1 \\ x_2 \end{bmatrix}} \tag{8}$$

$$\phi = \arctan\left(\frac{x_3}{r}\right) \tag{9}$$

$$\theta = -\arctan\left(\frac{x_2}{x_1}\right) \tag{10}$$

This model was implemented in MATLAB and independently verified using three-dimensional computer-aided design (CAD) software. The verification procedure involved creating a point at known azimuth and elevation angles. Planes with the angles α_0, α_1, and α_2 were created to simulate the laser fans. The planes were rotated about the z-axis until they were coincident with the point using geometric constraints. The angle of rotation could then be measured and used to calculate the time of rotation. These times were inputted to the MATLAB simulation and the output checked against the position of the original point. The model was shown to be valid in all quadrants and both hemispheres.

The uncertainty in the elevation and azimuth angles were propagated from the above model using Monte Carlo simulation. The nominal value and uncertainty for each variable in these equations was estimated as detailed in Table 1. The uncertainty in the rotational speed (ω) is dependent on a number of other assumptions

$$\omega = \frac{\alpha_3}{t_3} \tag{11}$$

where α_3 is the angular interval for counting the rotation of the head, and t_3 is the time between counts. Applying a first-order Taylor series approximation for the uncertainty in ω ($U\omega$) was propagated

Table 1 Variables used in mathematical model

Variable	Nominal	Standard uncertainty	Units	Description
t_0	0	10×10^{-9}	s	Time measurement strobe signal received by sensor
t_1	–	10×10^{-9}	s	Time measurement fan 1 signal received by sensor
t_2	–	10×10^{-9}	s	Time measurement fan 2 signal received by sensor
t_3	α_3/ω	10×10^{-9}	s	Time measurement for head to rotate by α_3
α_0	$\pi/2$	485×10^{-9}	rad	Azimuth angle of separation between fans
α_1	$\pi-\pi/6$	485×10^{-9}	rad	Angle of inclination of fan 1
α_2	$\pi/6$	485×10^{-9}	rad	Angle of inclination of fan 2
α_3	2π	485×10^{-9}	rad	Angular interval for counting the rotation of the head
ω	314	Equation (11)	rad/s	Angular velocity of rotating head
$\boldsymbol{n}_{1x}$	–	–	–	Vector normal to fan 1 when fan is aligned with x-axis
$\boldsymbol{n}_{2x}$	–	–	–	Vector normal to fan 2 when fan is aligned with x-axis
a_1	–	–	rad	Azimuth angle (from alignment with x-axis) of fan 1 t_1
a_2	–	–	rad	Azimuth angle (from alignment with x-axis) of fan 2 at t_2
$\boldsymbol{n}_{1T}$	–	–	–	Vector normal to fan 1 at t_1
$\boldsymbol{n}_{2T}$	–	–	–	Vector normal to fan 2 at t_2
$\boldsymbol{x}$	–	–	–	Vector on line through origin and target
Φ	–	–	rad	Elevation angle (+ve from x–y plane to +ve z)
θ	–	–	rad	Azimuth angle (+ve from +ve x to +ve y)

from the uncertainty in α_3 ($U\alpha_3$) and t_3 (Ut_3) and cancelling for t_3

$$U\omega = \frac{\omega}{\alpha_3}\sqrt{U\alpha_3^2 + \omega^2 \times Ut_3^2} \quad (12)$$

Based on a convergence study it was decided to run all simulations with 10 000 trials, which was regarded to be a reasonable compromise between accuracy and computational expense. Figure 3 shows how the accuracy of the simulation improves with the number of trials in the simulation. Unless otherwise indicated the nominal values given in Table 1 are used in all simulations.

Simulations were carried out with 156 different combinations of azimuth and elevation angles. The elevation angles ranged from -29° to 29° and the azimuth angles from 5° to 335°. The results of these simulations are shown in Figs 4(a) and (b). As would be expected considering the symmetry of the system the azimuth angle has no effect on the uncertainty in the measured angles. The elevation angle does have a noticeable effect on uncertainty. At extreme elevation angles (both positive and negative) the uncertainty in the elevation decreases while the uncertainty in the azimuth increases. Since the uncertainty in azimuth is consistently higher this indicates that it would generally be preferable to avoid measuring at extreme elevation angles.

Figure 5(a) shows the accuracy of the system plotted against the number of revolutions of the head per head speed calculation. This amounts to the number of revolutions over which the angular velocity of the head is averaged. Increasing the number of revolutions reduces the effect of timing error on calculated angular velocity. It can be seen that averaging the head speed over more than one revolution would have a negligible effect on the combined uncertainty.

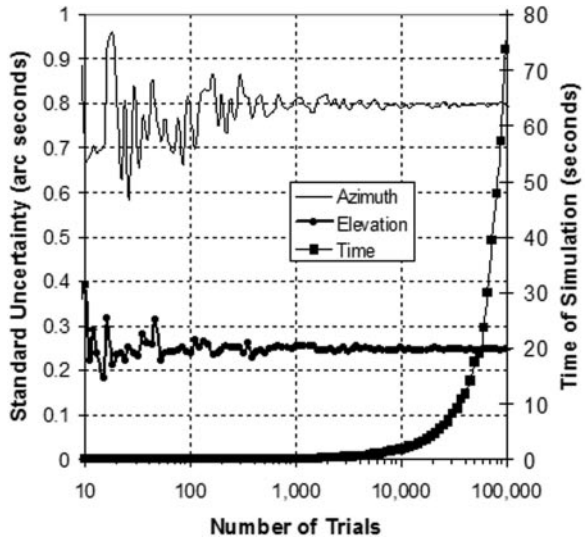

Fig. 3 Convergence of Monte Carlo simulation

Figure 5(b) shows that there is a linear increase in uncertainty as the angular velocity of the transmitter head is increased. This is explained by the uncertainty in timing being translated into a larger angle at greater speeds.

Figure 5(c) shows the effect of uncertainty in the measurement of the times t_0, t_1, t_2, and t_3 on the accuracy of the system. With timer uncertainties of greater than 1 ns there is clearly a relationship of the form $y = a \times x^k$. The flattening of the curve for values below 1 ns can be explained by the effect of the timer uncertainty becoming negligible and therefore other fixed uncertainties dominating.

Figure 5(d) shows the effect of uncertainty in the internal angles α_0, α_1, α_2, and α_3 on the uncertainty in the elevation angle. The uncertainty of the internal angles represents the accuracy with which the lasers are known to be spaced around the direction of rotation (α_0) and inclined to the horizontal (α_1 and α_2), and the accuracy with which the angular position (α_3) is known for the trigger which monitors the angular velocity of the rotating head. Surprisingly, the simulations show that it is possible to achieve higher accuracy in the measurement of elevation and azimuth than the system possesses in terms of these internal angles.

It can be seen from Figs 4(a) to 5(d) that for a given set of parameters, the uncertainty in azimuth is considerably higher than the uncertainty in elevation. The uncertainty in timing is very important and very low values of this parameter are required to obtain sensible values for combined uncertainties. It is difficult to extrapolate much more information than this from the simulations as there are a large number of variables whose values are unknown. It is important to stress that the actual values of the variables used in these simulations are unknown, and reasonable estimates have been used to demonstrate the simulated impact of certain parameters on measurement angles' uncertainties. There has also been no attempt to model the behaviour of the sensor, which will introduce additional uncertainties.

4 EXPERIMENTAL PROCEDURE

A simple test was devised to compare the azimuth measurement from the R-LAT with a reference angle established by use of a high-precision rotary table. The basic procedure is to place the transmitter on the rotary table with the sensor located at some fixed point and at an appropriate distance from the transmitter. An angle is measured using the R-LAT. The transmitter is then rotated through a known reference angle using the rotary table. Finally, a second angle is

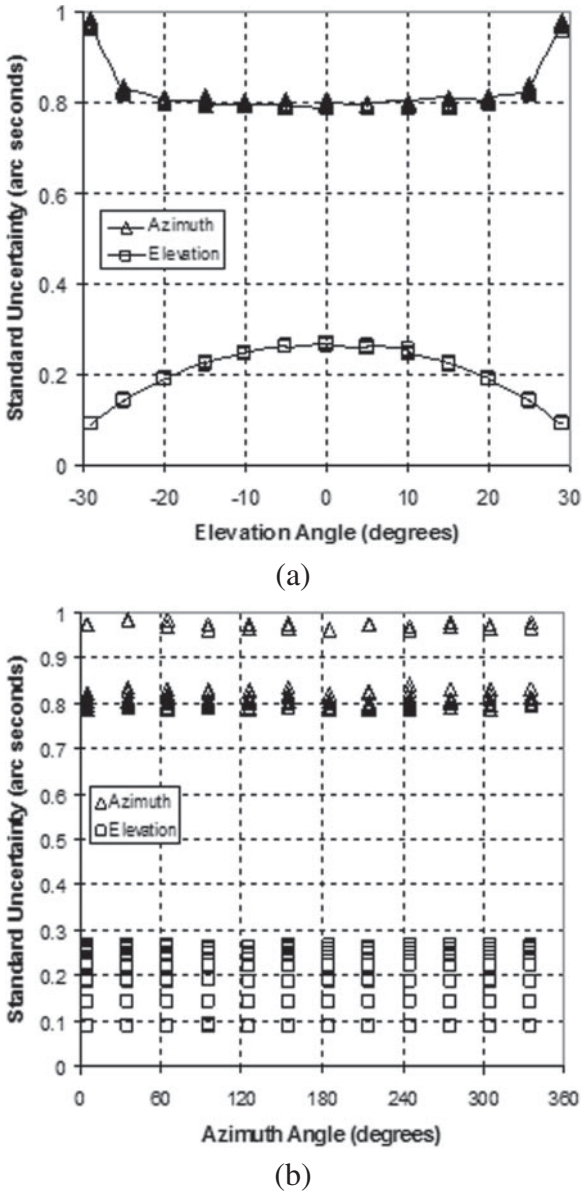

Fig. 4 Sensitivity of uncertainty in azimuth and elevation to: (a) the elevation angle; and (b) the azimuth angle

measured using the R-LAT. The difference between the two angles measured using the R-LAT can now be compared with the reference angle.

The actual tests were slightly more complicated than the basic procedure described above. First, it was important to ensure that the axis of rotation of the transmitter was coaxial with the rotation of the rotary table. For this purpose, a specially constructed reference cylinder was attached to the rotating head of the transmitter as shown in Fig. 6. The reference cylinder was attached in such a way that it could be moved around on the surface of the centring base and also jacked off the centring base so as to deviate slightly from the perpendicular in any direction.

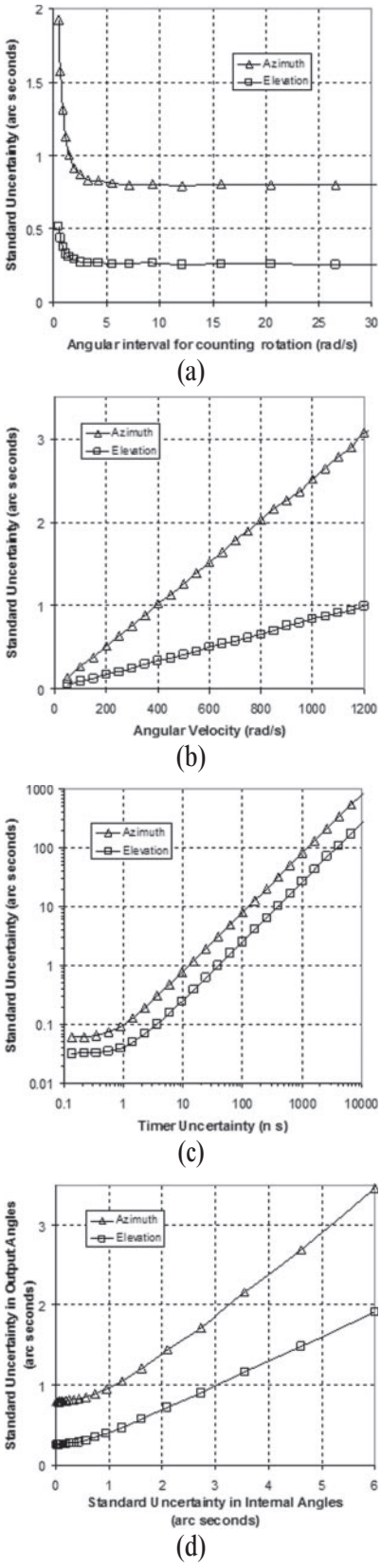

Fig. 5 Sensitivity of uncertainty in azimuth and elevation to: (a) the frequency of counting the transmitter head revolution (α_3); (b) the angular velocity of the transmitter head (ω); (c) the timer uncertainty; and (d) the uncertainty in internal angles

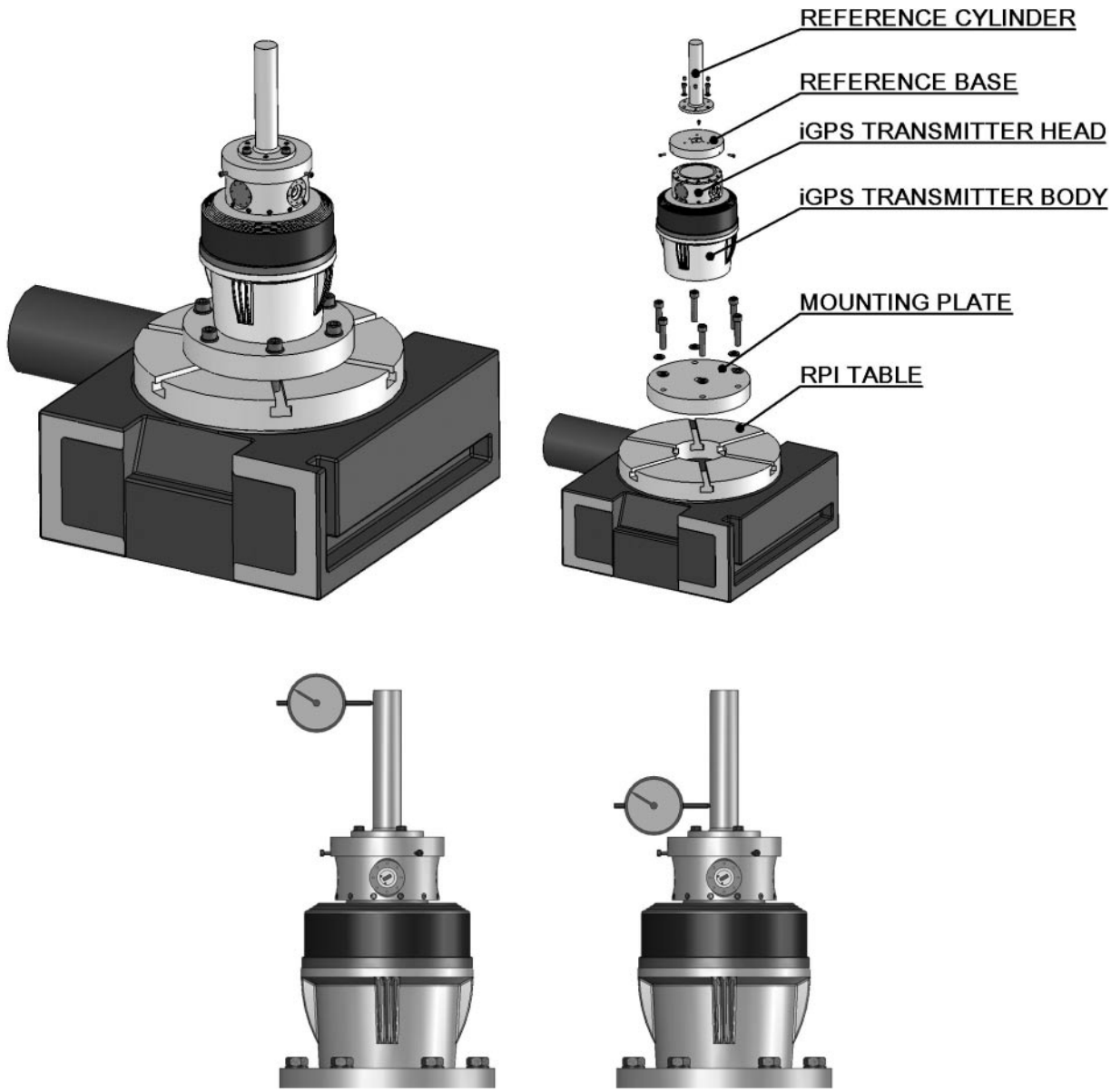

Fig. 6 Assembly of transmitter on rotary table

The reference cylinder was first positioned approximately concentric with the transmitter. A dial gauge was then used to measure the deflection of the reference cylinder as the head was slowly rotated. The reference cylinder was moved on the centring base according to the measurements, and in this way the reference was made concentric with the axis of rotation. The dial gauge was then moved to a position 100 mm further up on the cylinder to check the concentricity at a second point and therefore that the cylinder was parallel with the axis of rotation. Again the head was rotated and the cylinder was jacked off the surface according to the measurements made. The procedure was iterated a number of times. Both positions of the dial gauge are indicated in Fig. 6.

Having acquired a good reference for the axis of rotation, the procedure was repeated with the modification that the transmitter was moved in relation to the rotary table. In this way the axis of rotation of the transmitter was aligned with the axis of rotation of the rotary table.

It was decided to be impractical to carry out tests for the uncertainty in the elevation angle for a number of reasons.

1. Results of tests for the azimuth measurement capability detailed in section 6 show that the R-LAT probably has an uncertainty of equal to or better than the uncertainty in the reference angle. It has already been shown in section 3 that the uncertainty in elevation angle must be lower

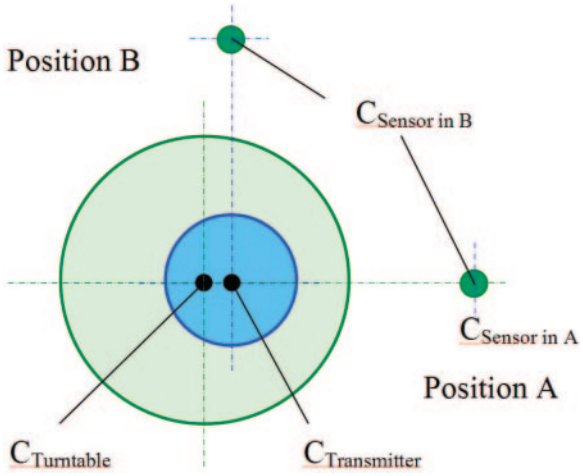

Fig. 7 Extreme orientations for concentricity error

than that in azimuth. We would, therefore, require an experimental setup that is more controlled than already achieved herein in order to derive any new information.

2. It would not be possible to simply rotate the transmitter through a known reference angle since changes in elevation angle would potentially also move the position of the rotating head within its bearings, invalidating the experiment.
3. The alternative to rotating the transmitter through a known reference angle would be to move the sensor through a known angle. Since this rotation would be taking place at some considerable range the only feasible way to construct such a reference angle would be through the measurement of three lengths to construct a triangle. These lengths would consist of the distance between the upper and lower sensor position and the ranges from the origin of the transmitter's internal coordinate system to the two sensor positions. Unfortunately the exact position of the origin of the origin is not known. It is only known to be somewhere on the axis of rotation of the head.

5 EXPERIMENTAL ERROR BUDGET

5.1 Uncertainty in angle due to lack of concentricity

The error in a single angle measurement due to a lack of concentricity depends on the orientation of the offset with respect to the angle. Figure 7 shows two possible orientations. In position A the offset does not result in any error while in position B the offset results in a maximum error given by

$$E\theta_{C-Max} = \tan^{-1}\left(\frac{E_C}{r}\right) \quad (13)$$

where $E\theta_{C-Max}$ is the maximum error for the single angle measurement, E_C is the offset in concentricity, and r is the radial distance from transmitter to sensor.

The error for a single measurement taken at any position is given by

$$E\theta_C = \sin(\theta_A) \times \tan^{-1}\left(\frac{E_C}{r}\right) \quad (14)$$

where θ_A is the angle between position A and the position at which the angle measurement is being made.

For a reference angle that is constructed by taking two angle measurements at different indexed positions on the rotary table, the maximum error would occur when this reference angle is evenly spaced about position A. The error in the reference angle is therefore given by

$$E\theta_{C-ref} = 2 \times \sin\left(\frac{\theta_{ref}}{2}\right) \times \tan^{-1}\left(\frac{E_C}{r}\right) \quad (15)$$

The expression for the error in the reference angle was used to find the uncertainty in this angle by assuming that the error in concentricity was zero, but with a known uncertainty. It is then possible to perform a Monte Carlo simulation. The measured deviations in concentricity were inputted to this simulation as uncertainties with rectangular distributions.

5.2 Uncertainty in angle due to instability of the sensor

The error in a single angle measurement due to the instability of the tripod holding the sensor is given by

$$E\theta_T = \tan^{-1}\left(\frac{E_T}{r}\right) \quad (16)$$

where E_T is the error in the position of the sensor due to movement in the tripod.

The error in a reference angle constructed by taking two angle measurements is given by

$$E\theta_{T-ref} = \tan^{-1}\left(\frac{E_{T1}}{r}\right) + \tan^{-1}\left(\frac{E_{T2}}{r}\right) \quad (17)$$

The expression for the error in the reference angle can be used to find the uncertainty in this angle in the same way as described in section 5.1. In this case, the uncertainty in E_T was assumed to be normally distributed with a standard deviation determined by measuring the position of a retroreflector mounted on the tripod using an interferometer.

5.3 Uncertainty in angle due to lack of parallelism

The error in the reference angle due to lack of parallelism between the axes of the rotary table and transmitter is somewhat more complicated. First, one needs to consider the error in a single angle measurement. The Cartesian miss will be zero when the measurement is taken at the same height as the intersection of the axes and will be constant at a fixed height above this intersection. This is illustrated in Fig. 8 where it can also be seen that for any height the miss will be zero when measuring in the direction of the offset and will reach maximum value when measuring perpendicular to the offset.

We can generalize the above statements to say that

$$M = \sin\theta_{\mathrm{B}} \times h \tan E_{\mathrm{P}} \tag{18}$$

where M is the Cartesian miss, θ_{B} is the azimuth angle at which the measurement is being taken relative to the direction of the offset, h is the height of the measurement above the intersection of the two axes of rotation, and E_{P} is the error in parallelism.

The height h is given by

$$h = r \tan\phi \tag{19}$$

where r is the range of the measurement and Φ is the elevation angle.

Substituting

$$M = \sin\theta_{\mathrm{B}} \times r \tan\phi \times \tan E_{\mathrm{P}} \tag{20}$$

The error in the azimuth angle for a single angle measurement $E\theta_{\mathrm{P}}$ is given by

$$E\theta_{\mathrm{P}} = \tan^{-1}\frac{M}{r} \tag{21}$$

Substituting and cancelling

$$E\theta_{\mathrm{P}} = \tan^{-1}(\sin\theta_{\mathrm{B}} \times \tan\phi \times \tan E_{\mathrm{P}}) \tag{22}$$

For a reference angle constructed by taking two angle measurements at different indexed positions on the rotary table, the maximum error would occur when this reference angle is evenly spaced about the direction of the offset. The error in the reference angle is therefore given by

$$E\theta_{\mathrm{P-ref}} = \tan^{-1}\left[\sin\left(\frac{\theta_{\mathrm{ref}}}{2}\right) \times \tan\phi \times \tan E_{\mathrm{P}}\right] - \tan^{-1}\left[\sin\left(\frac{-\theta_{\mathrm{ref}}}{2}\right) \times \tan\phi \times \tan E_{\mathrm{P}}\right] \tag{23}$$

where, θ_{ref} is the size of the reference angle, E is the elevation, and E_{P} is the error in parallelism

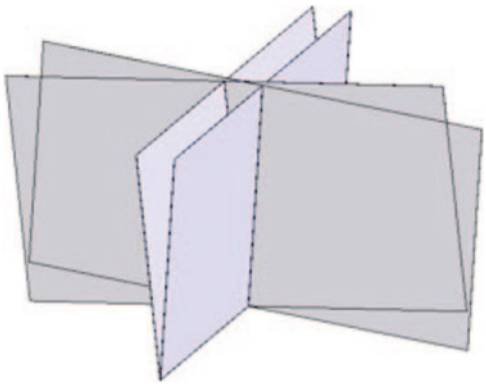

Fig. 8 Error due to lack of parallelism

As described above, the expression for the error in the reference angle was used to find the uncertainty in this angle using Monte Carlo simulation. The measured deviation in parallelism was inputted to the simulation as an uncertainty with a rectangular distribution.

5.4 Uncertainty in azimuth due to refractive changes

Temperature gradients in the air lead to distortion of laser propagation owing to changes in the refractive index of the air. Equations used to determine uncertainties due to these effects are documented in the ASME standard relating to laser trackers [**17**].

5.5 Combined uncertainty budget

The individual components of uncertainty in the reference angle were added in quadrature and then divided by the square root of two to give the error in a single angle (see Table 2).

6 EXPERIMENTAL RESULTS

The raw results for each test were processed as follows. Each individual stream of angle data was averaged over the specified time period to give a single angle reading. The difference between each pair of readings was then found to give a set of measurements of the reference angle (θ_{Mref}). For each data point 25 measurements of the reference angle were used to calculate the mean, standard deviation, and standard deviation of the mean. The difference between the actual reference angle and the mean was then divided by the standard deviation in the mean to give a 'z-score'; this was used to determine whether it was likely that the sample belonged to a population with a mean equal to the reference angle. The process is illustrated in Fig. 9.

Table 2 Uncertainty budget

Details of tests			Expanded uncertainty (in arc seconds) for reference angle due to uncertainty in:					
r	Φ	Ref angle	Table	⊕	//	Tripod	Refraction	Total expanded uncertainty for single angle
(mm)	(deg)	(deg)						
3995	0	1	0.467	0.002	0.00	0.511	0.041	0.49
6157	0	1	0.467	0.001	0.00	0.332	0.063	0.41
8434	0	1	0.467	0.001	0.00	0.242	0.087	0.38
10 605	0	1	0.467	0.001	0.00	0.193	0.109	0.37
13 406	0	1	0.467	0.000	0.00	0.152	0.138	0.36
4000	0	1	0.467	0.002	0.00	0.511	0.041	0.49
4000	4	1	0.467	0.002	0.01	0.511	0.041	0.49
4000	10	1	0.467	0.002	0.01	0.511	0.041	0.49
4000	16	1	0.467	0.002	0.02	0.511	0.041	0.49
4000	24	1	0.467	0.002	0.04	0.511	0.041	0.49
4000	28	1	0.467	0.002	0.04	0.511	0.041	0.49
4000	1	1	0.467	0.002	0.00	0.511	0.041	0.49
4000	1	2	0.467	0.003	0.00	0.511	0.041	0.49
4000	1	4	0.467	0.006	0.01	0.511	0.041	0.49
4000	1	8	0.467	0.013	0.01	0.511	0.041	0.49
4000	1	16	0.467	0.025	0.02	0.511	0.041	0.49
4000	1	32	0.467	0.049	0.04	0.511	0.041	0.49

In all tests it was found to be highly likely that the sample belonged to a population with a mean equal to the reference angle: z-values of less than 0.01. The uncertainty can therefore be expressed as simply the standard deviation, ignoring the deviation of the mean from the reference.

The uncertainty for each individual angle reading was calculated by assuming that the uncertainty in the first and second angle readings (θ_1 and θ_2) were equal so that the law of propagation of uncertainty [**20**] can be rearranged as

$$U\theta_{\text{Mref}} = \sqrt{U\theta_1^2 + U\theta_2^2}$$

However, $U\theta_1 = U\theta_2$

$$U\theta_{\text{Mref}} = \sqrt{2U\theta_1^2}$$

$$U\theta_1 = \frac{U\theta_{\text{Mref}}}{\sqrt{2}} \tag{24}$$

The data stream from the iGPS receiver consists of approximately 40 angle measurements per second. Normally, this data would be averaged to produce a more accurate result than given by simply using a single measurement. This is illustrated in Fig. 10(a); uncertainty in measurements can be seen to decrease rapidly as the sampling duration is increased up to approximately 0.5 s; the uncertainty then becomes more stable and only small improvements are seen beyond approximately 2 s. It is important to note that the lowest level of uncertainty seen is approximately 0.5″ which is of approximately the same magnitude as the uncertainty that is inherent in the experimental calibration. It is, therefore, likely that the actual uncertainty of the R-LAT continues to decrease to some lower value with increased sampling duration.

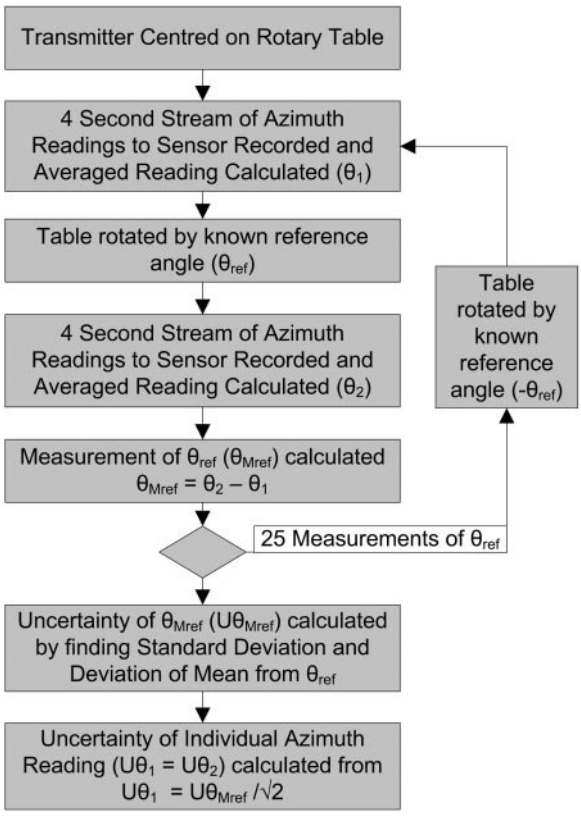

Fig. 9 Experimental process

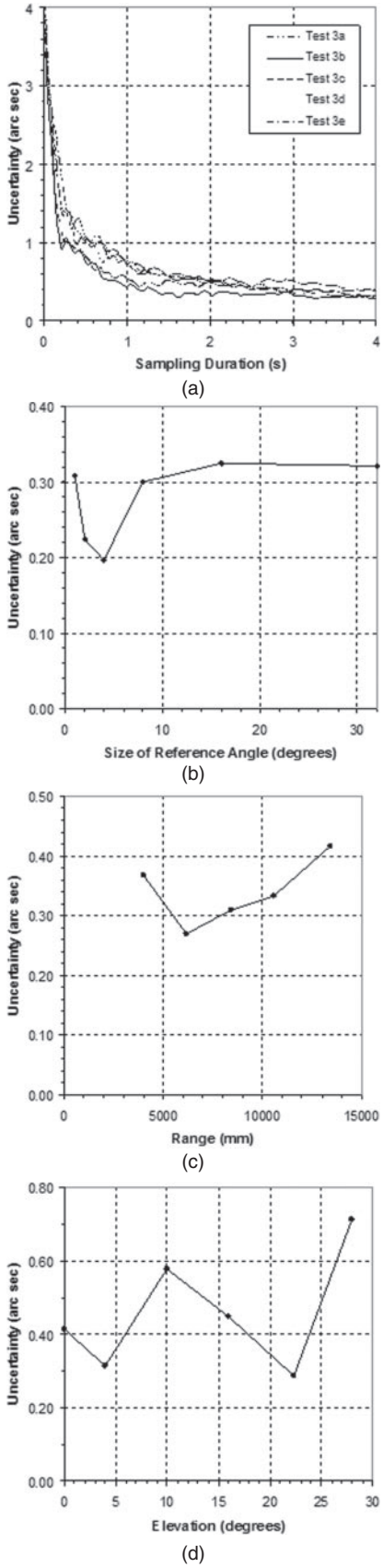

Fig. 10 Uncertainty in azimuth (95 per cent, confidence) against: (a) sample duration; (b) size of reference angle; (c) range; and (d) elevation

This type of behaviour where the accuracy improves dramatically when measurements are averaged over a period of time is typical with laser-based instruments. The causes are the averaging out of environmental disturbances such as vibration of the transmitter and sensor and refraction of the laser due to turbulence [**21**].

In total, 25 measurements of a reference angle were carried out with the transmitter and receiver at fixed positions, while increasing the size of the reference angle. This demonstrated that the uncertainty of measurements does not increase linearly with the size of the reference angle as illustrated in Fig. 10(b). A decrease in the uncertainty for references angles of 2 to 4° is most likely explained by the behaviour of the rotary table. The difference of 0.1″ is well within the uncertainty expected in the table. It was therefore decided to use a reference angle of 1° for all subsequent tests.

Repeated measurements taken at different ranges and elevations were used to plot the uncertainty against range (Fig. 10(c)) and the uncertainty against elevation (Fig. 10(d)).

The uncertainty was observed to be greater at a range of 4 m and then decreased at 6 m before increasing again steadily up to a range of 13 m. This behaviour could be explained by the dominance of Cartesian miss at close range and of refractive changes at greater ranges. This behaviour could also be explained by other sources.

No clear relationship was observed between the elevation angle and the uncertainty in azimuth measurement. The sharp increase in uncertainty for the extreme of 28° elevation shows some agreement with the mathematical model (Fig. 4(a)) but the increase at 10° is not explained by the model. There was some variation in the uncertainty at different points but this does not appear to be correlated with the elevation, and could be attributed to some other environmental factors. Possible environmental causes for this disturbance are reflections, interference from other light sources, and variations in the refractive index of air. It could also be explained by the uncertainty inherent to the rotary table.

7 CONCLUSIONS

It is possible to draw a number of useful conclusions from the experimental work carried out concerning the azimuth measurement capabilities of the R-LAT system.

1. Tests indicate a level of uncertainty that is at least as low as the 1″ claimed by the manufacturer.
2. The uncertainties measured are at approximately the same level as the total uncertainty for the

experimental calibration; it is therefore likely that the system could achieve a higher accuracy than the value measured.
3. In order to achieve this level of accuracy, measurements must be averaged over at least 1 s and preferably more than 2 s.
4. The uncertainty does not increase with the size of the angle being measured although the relationship was unclear.
5. The is no clear relationship between uncertainty and range or elevation.
6. There was considerable variation in uncertainty at different measurement positions possibly owing to reflections.

This work has provided valuable learning concerning verification of the iGPS system. Practical limitations have meant that we were not able to achieve an experimental calibration sufficiently more accurate than the instrument being verified. Furthermore, it was determined to be impractical to carry out verification of the elevation angle measurement capabilities of the instrument. Owing to these limitations we now feel that future efforts should be concentrated on directly verifying the coordinate measurement capability of the system with work currently scheduled in the area.

ACKNOWLEDGEMENTS

The work has been carried out as part of the EPSRC, IdMRC at the Mechanical Engineering Department of the University of Bath, under grant EP/E00184X/1. The authors wish to thank Ian Whitehead from Rotary Precision Instruments, Tom Hedges from Metris, and Peter Dunning from Bath University for their technical inputs.

REFERENCES

1 **Hedges, T. M., Takagi, H., Pratt, T.,** and **Sobel, M. J.** Position measurement system and method using cone math calibration. United States Patent US 6,535,282 B2 Mar. 18, 2003.
2 **Sharke, P.** Measuring across space and time; large-scale metrology moves GPS in out of the rain. *Mech. Engng*, 2003, **125**(1), 48.
3 **Sell, C.** On the right lines. *Engineer*, 2005, **293**(7680), 30.
4 **Djurdjanovic, D.** and **Ni, J.** Online stochastic control of dimensional quality in multistation manufacturing systems. *Proc. IMechE, Part B: J. Engineering Manufacture*, 2007, **221**, 865–880.
5 **Gottwald, R.** SPACE – an automated non-contact 3-D-measuring-system for industrial applications. Seventh International Conference on Robot Vision and Sensory Controls, Zurich, Switzerland, 2–4 Feb, 1988.
6 **Gilby, J. H.** and **Parker, G. A.** Laser tracking system to measure robot arm performance. *Sensor Rev.*, 1982, **2**(3), 180–184.
7 **Logsdon, T.** *The Navstar global positioning system*, 1992 (Chapman and Hall, London).
8 **Watson, J. T.** A new approach to large coordinate measurement using four tracking interferometers. In Proceedings of the Third International Precision Engineering Seminar, Interlaken, Switzerland, 1985, pp. 68–71 (Butterworths, London).
9 **Hughes, E. B., Wilson, A.,** and **Peggs, G. N.** Design of a high-accuracy CMM based on multi-lateration techniques. *Manuf. Technol.*, 2000, **49**(1), 391–394.
10 **Zhang, D., Rolt, S.,** and **Maropoulos, P. G.** Modelling and optimisation of novel laser multilateration schemes for high-precision applications. *J. Meas. Sci. Technol.*, 2005, **16**, 2541–2547.
11 **Maropoulos, P. G., Zhang, D., Rolt, S., Chapman, P.,** and **Rogers, B. C.** Integration of measurement planning with aggregate product modelling for spacecraft design and assembly. *Proc. IMechE, Part B: J. Engineering Manufacture*, 2006, **220**, 1687–1695.
12 **Sprent, A.** The Anglescan positioning system. The 25th Australian Survey Congress: Observing New Directions, Melbourne, Australia, 1983.
13 **Triggs, B., Mclauchlan, P., Hartley, R.,** and **Fitzgibbon, A.** Bundle adjustment – a modern synthesis. *Lect. Notes Comput. Sci.*, 1999, **1883**, 1–4.
14 **Brown, D. C.** Densification of urban geodetic nets. *Photogramm. Engng Remote Sens.*, 1977, **43**(4), 447–467.
15 **Hadem, I.** Bundle adjustment in industrial photogrammetry. *Photogrammetria*, 1981, **37**(2), 45–60.
16 ISO 10360-2:2002. *Geometric product specifications acceptance and reverification tests for coordinate measuring machines (CMMs) – part 2: CMMs used for measuring size*.
17 ASME B89.4.19. *Performance evaluation of laser-based spherical coordinate measurement systems*, 2006.
18 Industrial theodolites & total stations data sheet en.pdf. 2008, available from http://www.leica-geosystems.com/corporate/en/products/total_stations/lgs_4387.htm.
19 ISO 17123-1:2002. *Optics and optical instruments – field procedures for testing geodetic and surveying instruments – part 1: theory*.
20 PD 6461-3:1995. *General metrology. Guide to the expression of uncertainty in measurement (GUM)*.
21 **Bobroff, N.** Recent advances in displacement measuring interferometry. *Meas. Sci. Technol.*, 1993, **4**(9), 907–926.

APPENDIX

Notation

a_1, a_2	azimuth angle from alignment with x-axis of fan 1 at t_1 and fan 2 at t_2 respectively (radians)
h	height of sensor above x–y plane (m)

n_{1x}, n_{2x} vectors normal to fan 1 and fan 2 when respective fans are aligned with x–axis
n_{1T}, n_{2T} vectors normal to fan 1 at t_1 and fan 2 at t_2 respectively
r radial distance from transmitter to sensor (m)
t_0 time measurement of strobe signal being received by sensor (s)
t_1 time measurement fan 1 signal received by sensor (s)
t_2 time measurement fan 2 signal received by sensor (s)
t_3 time measurement for head to rotate by α_3 (s)
$\boldsymbol{x}$ vector on the line through origin and target
E_C error in concentricity between axis of transmitter and axis of rotary table (m)
E_P error in parallelism – the angle between the axis of the transmitter and the axis of the rotary table (radians)
E_T error in position of sensor due to movement in the tripod (m)
E_{T1}, E_{T2} error in position of sensor due to movement in the tripod for the first and second azimuth of the measurement of a reference angle θ_{ref} (m)
$E\theta_{C–Max}$ maximum error in azimuth due to deviation from concentricity for a single measurement (radians)
$E\theta_{C–ref}$ error in measurement of reference angle θ_{Mref} due to error in concentricity (radians)
$E\theta_P$ error in a single angle measurement due to error in parallelism (radians)
$E\theta_{P–ref}$ error in measurement of reference angle θ_{Mref} due to error in parallelism (radians)
$E\theta_T$ error in a single angle measurement due to instability of the tripod holding the sensor (radians)
$E\theta_{T–ref}$ error in measurement of reference angle θ_{Mref} due to movement in the tripod (radians)
M Cartesian miss (m)
Ua_3 uncertainty in the angular interval for counting the rotation of the head α_3 (radians)
Ut_3 uncertainty in the time measurement for t_3 (s)
$U\omega$ uncertainty in the angular velocity ω (rad/s)
α_0 azimuth angle of separation between fans (radians)
α_1 angle of inclination of fan 1 (radians)
α_2 angle of inclination of fan 2 (radians)
α_3 angular interval for counting the rotation of the head (radians)
θ azimuth angle (+ve from +ve x to +ve y) (radians)
θ_1, θ_2 first and second azimuth measurements respectively, used to make measurement of reference angle (radians)
θ_A angle between current azimuth angle and azimuth where error in concentricity aligns so as to result in no error in azimuth (radians)
θ_B angle between current azimuth angle and azimuth where error in parallelism aligns so as to result in no error in azimuth (radians)
θ_{Mref} measurement of reference angle made using R-LAT (radians)
θ_{ref} reference angle between two azimuth angles, measured using rotary table (radians)
Φ elevation angle (+ve from x–y plane to +ve z) (radians)
ω angular velocity of rotating head (rad/s)